JOURNAL OF MATERIALS SCIENCE 31 (1996) 3507–3512

A generalized plane strain technique for estimating effective properties of particulate metal matrix composites using FEM

N. RAMAKRISHNAN, A. M. KUMAR, B. V. RADHAKRISHNA BHAT
Computer Simulation Centre, Defence Metallurgical Research Laboratory, Kanchanbagh P.O., Hyderabad 500 058, India

A procedure to estimate the effective elastic moduli and coefficient of thermal expansion (CTE) of particulate-reinforced metal matrix composites (MMCs) using a two-dimensional finite element method is presented. The actual microstructural geometry of the composites with randomly distributed second-phase particles is incorporated in the model. A generalized plane strain technique, realistically to describe the three-dimensional behaviour, is also incorporated in the model. The elastic moduli and the CTE, estimated using this model, agree favourably with the experimental data. The technique is shown to be superior compared to the conventional two-dimensional plane stress and plane strain approximations. Also, the results indicate that the effect of the shape of the randomly distributed second-phase particles on the effective elastic moduli is insignificant. Although the procedure is demonstrated for particulate MMCs, it can be easily extended to many other materials as well.

1. Introduction

A number of studies, both analytical and numerical, have been reported in the literature for estimating the effective properties of multiphase composites in terms of size, shape, volume fraction and distribution of the constituent phases. Hashin [1] and Hashin and Shtrikman [2] developed a composite sphere model with which they derived the effective bulk modulus and bounds for the effective shear modulus. Hill [3] and Budiansky [4] independently presented a self-consistent model. Zimmerman [5] obtained the effective moduli of a matrix containing rigid inclusions based on the differential method established by Norris [6] and McLaughlin [7]. Mori and Tanaka [8] introduced an eigen strain method which was later improved by Benvensite [9]. Wu [10] generalized the self-consistent model for ellipsoidal inclusions. The majority of the analytical methods available today are only variants of the above models and a comprehensive overview is presented by Christensen [11]. Although the analytical models are attractive because they offer better physical insight, any attempt to extend them to complex geometries invariably leads to mathematical intractability.

Many of the numerical models [12–20] published so far, although FEM based, are restricted to unit-cell approaches in which the real structure is approximated to a periodic array of certain regular geometries. In the case of composites of aligned fibres this assumption can be considered reasonable. However, these models are not valid when the spatial and the size distribution of the reinforcement are random, as in particulate composites. In this context, we present a finite element-based numerical model that incorporates the complexities associated with the spatial and size distribution of the second phase and demonstrate the use of the model in estimating the effective elastic properties of particulate-reinforced metal matrix composites (MMCs). In this paper, we describe the method, specifically illustrating its use in determining the effective elastic modulus and the coefficient of thermal expansion.

2. Finite element model (FEM)

In this section, we describe the finite element model where we consider typical microstructural geometries of particulate MMCs with spherical as well as angular reinforcements distributed randomly. Also, we introduce a type of generalized plane strain method to treat the three-dimensional deformation by means of a two-dimensional approximation.

2.1. Geometrical characterization

Representative cross-sectional micrographs of a typical MMC reinforced with 20% volume fraction of circular and angular second-phase geometries are shown in Fig. 1a and b, respectively. In order to ensure a spatial random distribution, we employ the following procedure: it is well known that a perfectly random distribution of the second phase results in identical area and volume fractions. Here, we use the converse of this principle to establish the random

0022–2461

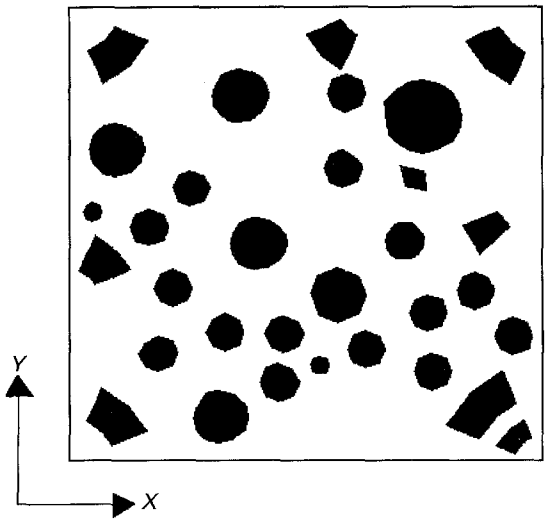

(a)

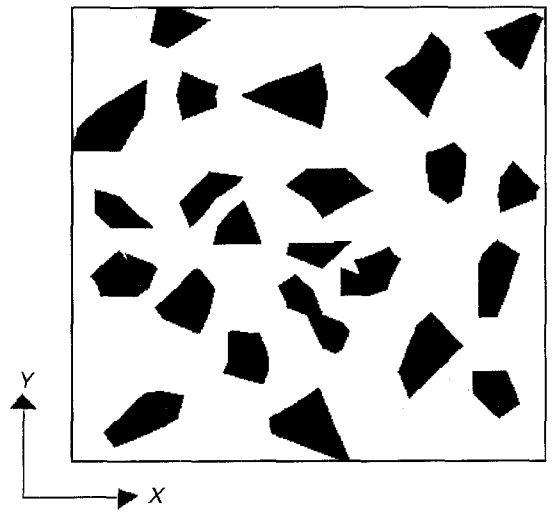

(b)

Figure 1 Representative cross-sectional micrographs of a typical MMC reinforced with 20% volume fraction of (a) circular and (b) angular particles.

distribution of the second phase. Initially, the second-phase particles are positioned at different locations in the matrix such that they appear random on a simple visual examination. Subsequently, this two-dimensional geometry is rotated about the X and Y axes to generate cylindrical volumes with toroidal second-phase particles and the volume fractions are computed. These volume fractions are compared with the area fraction and, depending on the difference, the second-phase particles are relocated in the matrix so as to reduce this difference to nearly zero. The repositioning is continued until the difference is reduced below a permissible level, which we chose to be 1%.

2.2. Mesh discretization

In order to generate the finite element grids corresponding to different volume fractions, as well as shapes of the second-phase particles, we use the master mesh concept outlined elsewhere [21, 22]. The master mesh, shown in Fig. 2, comprises constant

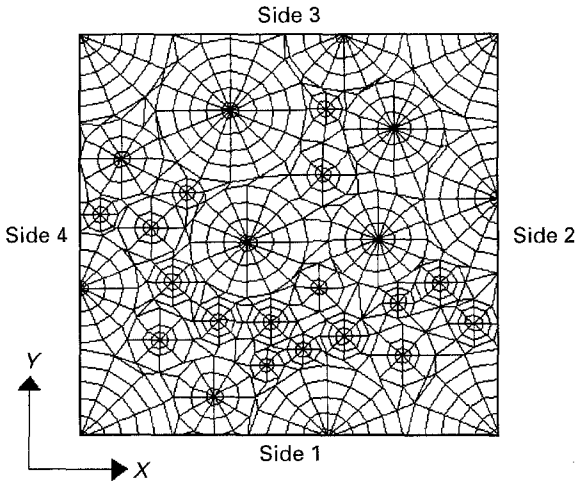

Figure 2 Master mesh for generating various microstructural morphologies.

strain triangular and quadrilateral elements. A variety of microstructural morphologies can easily be modelled using the master mesh by assigning the material properties of the second phase to selected elements. The matrix material properties are then assigned to the remaining elements. Using this procedure, the shape of the second phase, as well as its volume fraction, can be altered easily.

2.3. Boundary conditions

The estimation of the effective moduli involves determining the elastic response of the composite to externally applied loads which is accomplished by the following boundary conditions. The nodes along the bottom edge of the mesh (side 1 in Fig. 2) are fixed in the Y direction but allowed to move in the X direction. The nodes falling on the left edge of the mesh (side 4) are fixed in the X direction and are left free to move in the Y direction. A load is then applied to the mesh in the Y direction by displacing the nodes along the top edge of the mesh (side 3). Only small displacements are prescribed to avoid the onset of geometric and material non-linearities. This is necessary to ensure an accurate determination of the elastic modulus. The mesh is loaded specifically using the displacement–boundary conditions instead of force–boundary conditions to avoid numerically induced surface unevenness. For each of the volume fractions considered, the analysis is repeated for X-directional loading as well. The effective Young's modulus is then computed as the average of the two cases, that is, X and Y loading conditions. This is done in view of the small difference in the X and Y generated volume fractions. The effective bulk modulus, on the other hand, is computed by applying pressure in both X and Y directions simultaneously, using displacement boundary conditions as before. Independently computing the effective bulk modulus may appear to be a redundant step because one can obtain both the effective Young's modulus and the Poisson's ratio at the same time. However, we find the numerically induced error to be significant if we determine the Poisson's ratio by this

procedure. This aspect is discussed in Section 3.1 in detail. It is immaterial whether the loading is tensile or compressive and in this study we have chosen to impose compressive boundary conditions.

For determining the effective coefficient of thermal expansion, a small increase of temperature is imposed on all the elements, and the overall expansion of the composite is measured for the given CTEs of the individual phases. This is done with side-1 constrained in the y direction and side-4 constrained in the X direction to ensure the stability of the system.

2.3.1. The generalized plane strain method

The FEM analysis of particulate-reinforced composites should strictly be three-dimensional. However, any three-dimensional analysis, in addition to being cumbersome, demands large computing resources. On the other hand, two-dimensional approximations such as plane strain or plane stress, are inadequate. As a compromise, we introduce a generalized plane strain method.

It is known that the plane strain or the plane stress deformation is modelled by setting the strain or the stress in the Z-direction to zero. In generalized plane strain methods, a definite Z-directional strain is imposed and the Z-strain is chosen depending on the application. In our case, the magnitude and the sign of the Z-strain at any location of a particular constituent phase are forced to be the same as the average strain of that phase in the lateral direction. That is, the Z-directional strain in the ith phase for the loading in the Y-direction is

$$(\varepsilon_Z)^i = \frac{\sum_{j=1}^{n} V_j^i (\varepsilon_x)_j^i}{\sum_{j=1}^{n} V_j^i} \tag{1}$$

where n is the total number of elements representing the ith phase. In this method, in addition, the out-of-plane shear stress and strain terms are ignored, similar to the plane stress and the plane strain approximations. The algebraic details regarding the reduction of the three-dimensional constitutive matrix to the generalized plane strain matrix are provided in the Appendix.

If a homogeneous and isotropic material is loaded uniaxially, it produces identical lateral strains. Similarly, any composite which is statistically homogeneous and isotropic will also produce equal lateral global strains, even though the strain at any particular location depends on the microstructural morphology and the elastic properties of the constituent phases. The present generalized plane strain method forces the average strain in one lateral direction to be the same as that in the other lateral direction for each constituent phase independently. This not only ensures the lateral strains to be the same at the global level but also allows the Z-strain to be different for different phases depending on their elastic moduli. In the limiting case of the second-phase volume fraction approaching zero, the generalized plane strain approaches the plane stress condition.

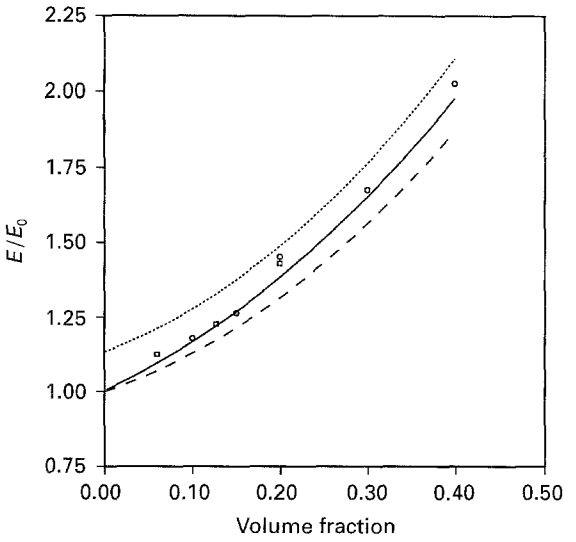

Figure 3 Comparison of (——) the generalized plane strain estimates of the effective Young's modulus with (· · ·) plane strain, (- - -) plane stress results and experimental data (□) [26], (○) [27].

2.4. Material properties [23–25]

Young's modulus, Poisson's ratio and CTE of the matrix (7075-T6 aluminium alloy) are 69 GPa, 0.33 and $23.4 \times 10^{-6}/°C$, whereas for the second phase (SiC particulate) these are 460 GPa, 0.18 and $4.7 \times 10^{-6}/°C$, respectively.

3. Results and discussion

The results of the model are compared with some of the experimental data [26, 27] as well as the analytical ones.

3.1. Effect of boundary conditions

The effective Young's modulus is computed as the ratio of the average stress over the cross-section of the grid to the average applied strain. The modulus is normalized with respect to the matrix elastic modulus, E_0, and then plotted as a function of the volume fraction of the second phase for circular particle geometry as shown in Fig. 3. In this figure, the results of the generalized plane strain method are compared with those of the plane stress and the plane strain methods as well as the experimental data. The experimental data and the generalized plane strain estimates of our model fall in between the plane stress and the plane strain values. This is expected because the plane stress and the plane strain assumptions constitute two extremes in approximating the three-dimensional deformation. The results show that the generalized plane strain technique yields better estimates of the effective Young's modulus than the conventional plane stress or plane strain approximations.

The effective Poisson's ratio is computed by two different methods. In the first method, a uniaxial strain is applied to the finite element mesh and the Poisson's ratio is directly calculated as the ratio of the average lateral strain to the applied axial strain and the effective Young's modulus as the ratio of the average stress

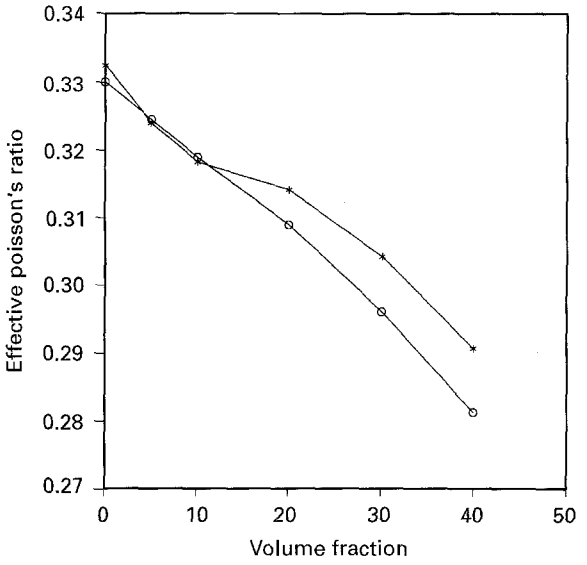

Figure 4 Variation of the Poisson's ratio with volume fraction of angular second-phase particles computed by two different methods: (*) average strains, (○) effective bulk modulus.

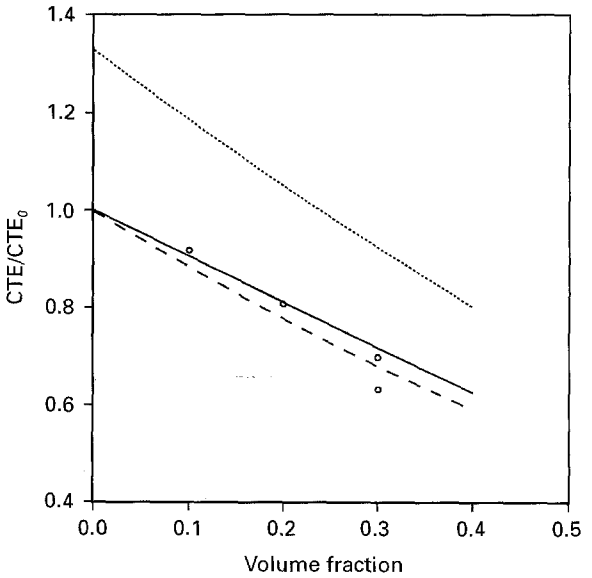

Figure 5 Comparison of (———) the generalized plane strain estimates of the effective coefficient of thermal expansion with (· · ·) plane strain, (- - -) plane stress results and (○) experimental data.

to the applied strain. In the second method, a biaxial compression in the X and Y directions is applied to the grid. The generalized plane strain method converts the biaxial compression into a three-dimensional hydrostatic compression by forcing the Z-strain to equal the X or Y strains for each phase. In this case, the bulk modulus is computed as the ratio of the hydrostatic stress to the volumetric strain. Subsequently, the Poisson's ratio is determined using the Young's modulus of the first method and the bulk modulus. The Poisson's ratios thus obtained using these two methods are shown in Fig. 4. The results indicate that the Poisson's ratio values computed using the first method show an erratic variation, whereas those of the second method exhibit negligible scatter. This, we feel, is due to the better numerical stability owing to the additional kinematic constraints imposed in the second method. Therefore, the second method is recommended for a more accurate determination of the effective Poisson's ratio, although it involves two steps.

The effective CTE of the composite is shown in Fig. 5. The experimental results agree favourably with the results of the generalized plane strain method. In contrast to the case of the effective elastic modulus, here the experimental results are close to the plane stress curve and the results of the generalized plane strain technique obey this trend as well.

3.2. Effect of particle shape

The results indicate negligible dependence of the effective moduli on the shape of the second-phase particles. This is illustrated in Fig. 6 where the bulk and the shear moduli are plotted for the cases of circular and angular particles. The average difference in the effective modulus for these two cases is less than 1%. Nevertheless, we found a significant difference in the stress distribution between the circular and the angular particle geometries for the same loading conditions. While the stress gradients are steep adjacent to the sharp corners of the angular particles, these are less pronounced around the circular particles. However, interestingly, the average stresses in both the cases are close to each other, which is a result of the random orientation and distribution of the second-phase particles. Therefore, we conclude that the shape of the particles has little effect on the elastic moduli, provided the structure is statistically homogeneous and isotropic with a perfectly bonded [28] particle matrix interface. On the other hand, the unit-cell models may predict an effect of the shape on the elastic moduli because the periodic array of the unit cells does not correspond to statistically isotropic conditions.

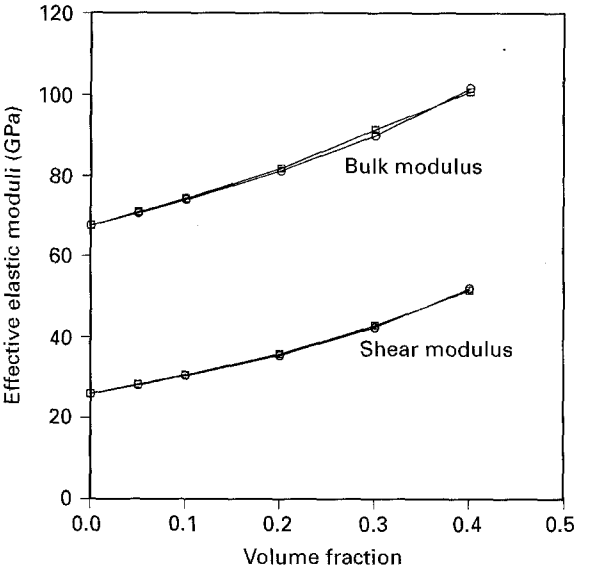

Figure 6 Effect of particle shape on the effective bulk and shear moduli for (○) circular and (□) angular particles.

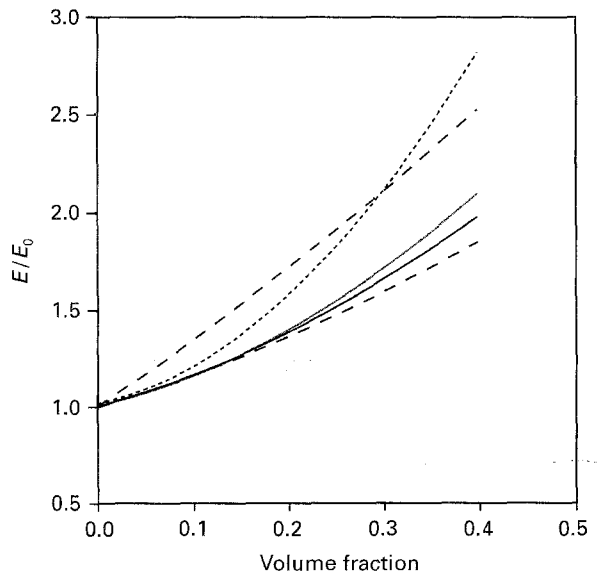

Figure 7 Comparison of (———) the generalized plane strain estimates with a few analytical estimates: (– – –) composite sphere method, (— — —) differential method, (· · ·) self-consistent method.

3.3. Comparison with analytical models

The FEM results are now validated with those of the composite sphere method [1, 2], the self-consistent method [3, 4] and the differential method [5–7], as shown in Fig. 7. This model is much more general compared to the analytical procedures and has a much wider applicability although, in this study, we have restricted ourselves to only the elastic moduli and CTE of particulate-reinforced MMCs. In contrast to the well-explored analytical methods, this technique is still in its early stages and thus offers a novel way of studying complex microstructural geometries. For example, the introduction of a particular type of shape, spatial and orientation distribution or clustering, is a simple extension of the present model which cannot be easily incorporated in any of the analytical methods. In addition, geometrical and material complexities such as non-linearity, etc., can also be easily incorporated in this method.

3.4. Limitations

Currently, the main limitation of the present model is that the particle–matrix interface is assumed to be perfectly bonded. Introducing the interfaces essentially involves finer discretization at the particle boundaries and this results in a prohibitively large problem size. More importantly, a rigorous description of the interface for the purposes of incorporation in the FEM procedures is still not available.

4. Conclusion

A general finite element model that describes elastic deformation of the real microstructures is presented specifically illustrating its use in determining the effective elastic moduli and coefficient of thermal expansion of particulate MMCs. The model takes into account the parameters such as spatial distribution, shape and volume fraction of the second phase with least idealizations. A master mesh concept is used for generating a variety of microstructural morphologies. A generalized plane strain approach is proposed and verified using available experimental results. The predicted elastic moduli and the coefficient of thermal expansion compare well with those from the published experimental data, as well as a few analytical estimates.

Acknowledgements

The authors thank the Director, DMRL, for encouragement, Mr Rakesh Sharma for assistance with computer modelling, and Mr P. Narsi Reddy for help in the preparation of the manuscript. N.R. acknowledges useful discussions with Dr V. S. Arunachalam, Senior Visiting Professor, CMU, Pittsburgh.

Appendix

The three-dimensional linear elastic constitutive equation, with the out-of-plane shear terms ignored, is

$$\begin{Bmatrix} \Delta\sigma_x \\ \Delta\sigma_y \\ \Delta\sigma_z \\ \Delta\tau_{xy} \end{Bmatrix} = \begin{bmatrix} C_{11} & C_{12} & C_{13} & C_{14} \\ C_{21} & C_{22} & C_{23} & C_{24} \\ C_{31} & C_{32} & C_{33} & C_{34} \\ C_{41} & C_{42} & C_{43} & C_{44} \end{bmatrix} \begin{Bmatrix} \Delta\varepsilon_x - \Delta\varepsilon_x^0 \\ \Delta\varepsilon_y - \Delta\varepsilon_y^0 \\ \Delta\varepsilon_z - \Delta\varepsilon_z^0 \\ \Delta\gamma_{xy} - \Delta\gamma_{xy}^0 \end{Bmatrix} \tag{A1}$$

where $\Delta\sigma$ and $\Delta\varepsilon$ are incremental normal stress and strain components, and $\Delta\tau$ and $\Delta\gamma$ are shear components. In the case of the generalized plane strain condition, we impose

$$\Delta\varepsilon_z = \varepsilon^* \tag{A2}$$

where ε^* has a definite value depending on the application. Substituting Equation A2 into Equation A1, we get

$$\begin{Bmatrix} \Delta\sigma_x \\ \Delta\sigma_y \\ \Delta\tau_{xy} \end{Bmatrix} = \begin{bmatrix} C_{11} & C_{12} & C_{14} \\ C_{21} & C_{22} & C_{24} \\ C_{41} & C_{42} & C_{44} \end{bmatrix} \begin{Bmatrix} \Delta\varepsilon_x \\ \Delta\varepsilon_y \\ \Delta\gamma_{xy} \end{Bmatrix} + \begin{Bmatrix} (-\psi_x + C_{13}\varepsilon^*) \\ (-\psi_y + C_{23}\varepsilon^*) \\ (-\psi_{xy} + C_{43}\varepsilon^*) \end{Bmatrix} \tag{A3}$$

where

$$\begin{Bmatrix} \psi_x \\ \psi_y \\ \psi_{xy} \end{Bmatrix} = \begin{bmatrix} C_{11} & C_{12} & C_{13} & C_{14} \\ C_{21} & C_{22} & C_{23} & C_{24} \\ C_{41} & C_{42} & C_{43} & C_{44} \end{bmatrix} \begin{Bmatrix} \Delta\varepsilon_x^0 \\ \Delta\varepsilon_y^0 \\ \Delta\varepsilon_z^0 \\ \Delta\gamma_{xy}^0 \end{Bmatrix} \tag{A4}$$

When $\varepsilon^* = 0$, the equation reduces to the plane strain method.

References

1. Z. HASHIN, *J. Appl. Mech.* **29** (1962) 143.
2. Z. HASHIN and S. SHTRIKMAN, *J. Mech. Phys. Solids* **11** (2) (1963) 127.

3. R. HILL, *ibid.* **13**(4) (1965) 213.
4. B. BUDIANSKY, *ibid.* **13**(4) (1965) 223.
5. R. W. ZIMMERMAN, *Mech. Mater.* **12** (1991) 17.
6. A. N. NORRIS, *ibid.* **4** (1985) 1.
7. McLAUGHLIN, *Int. J. Eng. Sci.* **15** (1977) 237.
8. T. MORI and K. TANAKA, *Acta Metall.* **21** (1973) 571.
9. Y. BENVENSITE, *Mech. Mater.* **6** (1987) 147.
10. T. T. WU, *Int. J. Solids Struct.* **2**(1) (1966) 1.
11. R. M. CHRISTENSEN, *J. Mech. Phys. Solids* **38** (1990) 379.
12. T. CHRISTMAN, A. NEEDLEMAN and S. SURESH, *Acta Metall.* **37** (1989) 3029.
13. V. TVERGAARD, *ibid.* **38** (1990) 185.
14. J. R. BROEKENBROUGH, S. SURESH and H. A. WIENECKE, *ibid.* **39** (1991) 735.
15. G. BAO, J. W. HUTCHINSON and R. M. McMEEKING, *Acta Metall. Mater.* **39** (1991) 1871.
16. N. SHI, B. WILNER and R. J. ARSENAULT, *ibid.* **4** (1992) 2841.
17. I. DUTTA, J. D. SIMS and D. M. SEEGENTHALER, *ibid.* **41** (1993) 885.
18. M. Y. HE, A. G. EVANS and W. A. CURTIN, *ibid.* **41** (1993) 871.
19. Y.-L. SHEN, M. FINOT, A. NEEDLEMAN and S. SURESH, *ibid.* **42** (1994) 77.
20. K. S. RAVICHANDRAN, *ibid.* **42** (1994) 1113.
21. N. RAMAKRISHNAN, H. OKADA and S. N. ATLURI, *ibid.* **39** (1991) 1297.
22. N. RAMAKRISHNAN and V. S. ARUNACHALAM, *J. Am. Ceram. Soc.* **76** (1993) 2745.
23. "Metals Handbook", "9th Edn," Properties and Selection: Non-ferrous alloys and Pure Metals" (American Society for Metals, 1979).
24. E. A. Brandels (ed.), "Smithells Metals Reference Handbook", 6th Edn (Butterworths, 1983).
25. ALCOA (Aluminum Company of America) "Aluminum Handbook" (1967).
26. D. L. McDANELS, *Metall. Trans.* **16A** (1985) 1105.
27. J. LLORCA, S. SURESH and A. NEEDLEMAN, *ibid.* **23A** (1992) 919.
28. R. MITRA, W. A. CHIOU, M. E. FINE and J. R. WEERTMAN, *J. Mater. Res.* **8** (1993) 2380.

Received 10 April
and accepted 25 October 1995